Appl. Math. Mech. -Engl. Ed., **47**(8), 1723–1746 (2026)

APPLIED MATHEMATICS AND MECHANICS (ENGLISH EDITION)

https://doi.org/10.1007/s10483-026-3414-8

End-to-end analysis of vibration of time-varying mass systems*

Kai WANG[1], Ao CHENG[1], Tingting CHEN[2], Jiaxi ZHOU[1], Zhuang LI[1], Shengtao ZHANG[3], Li CHENG[4,†]

1. College of Mechanical and Vehicle Engineering, Hunan University, Changsha 410082, China;
2. School of Mechanical and Intelligent Manufacturing, Central South University of Forestry & Technology, Changsha 410004, China;
3. College of Mechanical Engineering, Hunan University of Science and Technology, Xiangtan 411201, Hunan Province, China;
4. Department of Mechanical Engineering, The Hong Kong Polytechnic University, Hong Kong, China

(Received Feb. 25, 2026 / Revised May 18, 2026)

Abstract Vibration systems with time-varying mass are prevalent in engineering practice, exemplified by rockets with fuel depletion, vehicles with changing mass, and systems with cable-hoisted payloads. However, progress has been constrained by the lack of an end-to-end approach capable of integrating modeling, closed-form analysis, numerically stable calculations, and isolation design. Focusing on a typical system involving rocket fuel combustion with linear mass depletion, we first derive the equations of motion from the momentum theorem. A parameter transformation, constructed via the method of undetermined coefficients, converts the time-varying differential equation into a standard Bessel equation, yielding a closed-form analytical solution. To achieve reliable numerical solutions, a strategy combining variable upper-limit integration with grid-search-optimized lower bounds is deployed to replace indefinite integrals, thereby overcoming non-integrable products of Bessel functions. Benchmark comparisons with harmonic excitations show excellent agreement, validating the formulation and solution scheme. Building on the closed-form response, an end-to-end vibration isolation workflow is established via transmissibility and isolation failure-time-threshold (FTT) metrics, allowing for the selection of stiffness based on the instantaneous frequency ratio throughout the mass variation process. The resulting framework provides a general analytical tool for linear differential equations with time-varying mass and a practical pathway for vibration isolation design in mass-varying structures, with special relevance to aerospace applications.

* Citation: WANG, K., CHENG, A., CHEN, T. T., ZHOU, J. X., LI, Z., ZHANG, S. T., and CHENG, L. End-to-end analysis of vibration of time-varying mass systems. *Applied Mathematics and Mechanics* (*English Edition*), **47**(8), 1723–1746 (2026) https://doi.org/10.1007/s10483-026-3414-8

† Corresponding author, E-mail: li.cheng@polyu.edu.hk

Project supported by the National Key R&D Program of China (No. 2024YFB3408701), the National Natural Science Foundation of China (Nos. 12272129 and 12472010), the Natural Science Foundation of Hunan Province of China (Nos. 2024JJ4004 and 2024JJ3003), and the Fundamental Research Funds for the Central Universities of China

Key words vibration isolation, time-varying mass, Bessel equation, variable upper-limit integration

Chinese Library Classification O322
2020 Mathematics Subject Classification 34C05, 33C10, 70J30

1 Introduction

Many engineering dynamical systems can be modeled using linear differential equations with constant coefficients, which have been extensively used to address a wide range of theoretical and practical problems. However, numerous real-life systems and complex engineering phenomena impose the need to address differential equations with time-varying parameters[1–3]. Typical examples arise in variable-mass rotors in textile machinery, which are critical for winding tape fabrics and often exhibit excessive vibration at high speeds due to mass variation[4–5]. Rocket-burning fuel during launch is another salient example. Whether time-varying mass effects should be explicitly incorporated in the dynamic analysis primarily depends on the relative rate and magnitude of mass change. When both the net mass variation and changing rate are sufficiently small, the resulting dynamic coupling can be regarded as a perturbation, justifying the ignorance of its influence on the overall motion such as in ordinary automobiles despite the existence of fuel consumption. By contrast, when a system undergoes substantial mass variation over a short time interval, the time-varying mass effect becomes a dominant factor, exemplified by launch vehicles in which fuel constitutes a large portion of the total mass, and its rapid consumption during combustion can significantly alter the vibration characteristics[6–10]. Additional engineering scenarios involving time-dependent mass and stiffness include stiffness degradation due to gear wear, mass and stiffness variations caused by coating wear in blade-casing systems, motion of robotic arms on space stations, deployment of spacecraft solar panels, and extension of retractable wings[11–18]. In all these cases, time-varying parameters not only alter the intrinsic dynamic properties of the system, often yielding governing equations with time-dependent coefficients, but also can themselves become a primary source of excessive vibration. Consequently, the analysis and control of such system vibrations are of considerable practical importance[19–22].

Research on single-degree-of-freedom (SDOF) systems with time-varying parameters, particularly time-varying mass, has attracted sustained attention. Several studies have investigated free vibration in systems with gradually decreasing mass[23–27]. Li[28–29] derived the governing equations using the momentum theorem and obtained analytical solutions for both free and forced vibrations under exponential mass variation. Through tactical functional transformations, these studies transformed the original equations into solvable canonical forms to obtain closed-form analytical solutions, which have also been effectively used to analyze the transient dynamics of deployable/retractable continuous structures[30]. In parallel, advanced mathematical frameworks, such as asymptotic theories for time-varying integro-differential systems, continue to be developed to tackle inherent analytical intractability[31]. Other studies dealt with specific temporal variation patterns of parameters, such as power-lawed, exponential, or periodically piecewise-defined mass profiles, to derive exact solutions for particular classes of problems[32–34]. These studies have laid an important mathematical foundation for understanding the dynamics of time-varying mass systems.

In parallel, significant effort has been devoted to developing control strategies and computational frameworks capable of handling time-varying parameters. For vibration suppression, adaptive control algorithms and fuzzy-logic-based strategies have been proposed to accommodate non-stationary excitations and parametric uncertainties[35–37]. Liu et al.[38] highlighted the strategic importance of variable-stiffness isolators in spacecraft. Similarly, recent analytical investigations into quasi-zero stiffness systems, viscoelastic metamaterials for integrated vibration isolation[39] and energy harvesting[40–42], along with novel nonlinear structural designs such as nonlinear energy sinks[43–44] and multistable energy harvesters[45–46], have further validated the effectiveness of nonlinear stiffness regulation in enhancing low-frequency performance[47–50]. For systems involving moving components, such as elevator traction systems and flexible lifting structures, time-varying structural mechanics models have been employed to cope with dynamic fluctuations in mass and stiffness[51–52]. From a computational perspective, several studies have explored time-domain piecewise calculation schemes and proper orthogonal decomposition (POD) techniques to reduce the numerical cost associated with solving non-homogeneous equations with time-varying coefficients[53–54].

More recently, with the rapid advancement of metastructures[55], the exploration of time-dependent physical properties has expanded from macroscopic mechanical systems to the frontier of wave manipulation, giving rise to the emerging field of time-varying metamaterials. Unlike conventional metamaterials that rely solely on spatial topological design, time-varying (or space-time) metamaterials leverage time as an additional design dimension to break traditional constraints related to energy and momentum conservation, thereby enabling exotic phenomena such as non-reciprocal wave propagation and "four-dimensional optics"[56–57]. For instance, Huang and Zhou[58] achieved non-reciprocal mechanical wave propagation by introducing rotating mass blocks to produce periodically varying effective inertial mass. Similarly, Liu et al.[59] utilized self-reconfigurable virtual resonators to achieve autonomous modulation of stiffness and damping, demonstrating notable potential in pulse shaping and spectral control. These studies at the sub-wavelength scale primarily exploit time-varying parameters to realize specific functional responses of metamaterials. However, the fundamental dynamic behavior and vibration control of time-varying parameter systems, particularly those with time-varying mass, have received far less attention.

Despite the aforementioned progress, existing literature has several notable limitations. First, many of the available analytical solutions rely on specific functional forms of mass variation, and offer limited physical transparency, which restricts their applicability in real engineering problems. Second, while extensive research has been conducted on free vibration or particular forced-vibration configurations, relatively few studies have addressed more general and practically relevant scenarios involving linear or piecewise-continuous mass variation under realistic excitation conditions[60]. More importantly, a large portion of previous work has focused primarily on mathematical solvability, with insufficient attention paid to the vibration isolation performance and dynamic response characteristics under time-varying conditions. As a result, physical insights into how time-dependent parameters, especially mass depletion, affect transmissibility and isolation effectiveness remain obscure, offering limited guidance for engineering design[61].

To bridge these gaps, the present study systematically investigates systems with linearly decreasing mass, with particular emphasis on vibration isolation performance under sinusoidal excitations, representative of engine and aerodynamic loads[62–64]. The primary objective is to obtain an analytical solution for the equation of motion of a variable-mass system that is both mathematically tractable and physically interpretable. By employing Lagrange's equations together with variable upper-limit integration techniques, a closed-form solution for the forced-vibration response is derived. Beyond mathematical solvability, this study explicitly evaluates vibration transmissibility and isolation effectiveness under time-varying conditions, thereby providing direct performance-oriented insights. The proposed methodology, which is grounded in calculus-based concepts, is expected to be extendable to other types of mass-variation laws. In contrast to the purely numerical approaches commonly adopted when analytical solutions are unavailable, the present work offers a closed-form solution through suitable equation transformations, yielding a deeper understanding of the underlying dynamics. Numerical simulations are further conducted to verify the consistency between the analytical solution and approximate numerical results, demonstrating both the effectiveness and engineering relevance of the method. Therefore, this study not only provides a rigorous analytical framework for the design and validation of isolators operating in mass-varying environments, but also offers practical guidance, while holding broader theoretical significance for this class of time-varying differential equations.

The remainder of this paper is organized as follows. Section 2 establishes a theoretical model for a general SDOF system with linearly decreasing mass. Section 3 transforms the governing equation into a Bessel-type form, and presents the derivation of the closed-form analytical solution, along with the discussion on the key assumptions and mathematical techniques involved. Section 4 analyzes the performance of time-varying mass-spring vibration isolators, examining transient isolation performance under different stiffness configurations and elucidating the fundamental relationships between dynamic responses and design parameters. Section 5 concludes the study by summarizing the main findings and outlining potential extensions of the present work.

2 Dynamics of a time-varying mass system

Newton's momentum theorem is used to model the dynamics of an SDOF system with time-varying parameters, as schematically illustrated in Fig. 1.

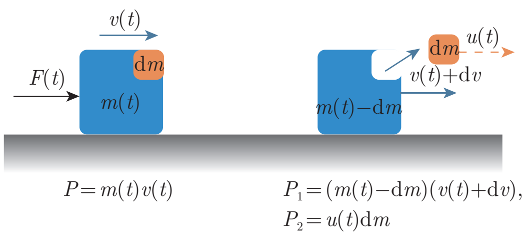

Fig. 1 Schematic of Newton's momentum theorem (color online)

By analyzing the momentum change of the variable-mass system over an infinitesimal time interval $\mathrm{d}t$, the general governing equation is formulated as follows:

$$m(t)\frac{\mathrm{d}^2x(t)}{\mathrm{d}t^2}+\frac{\mathrm{d}m(t)}{\mathrm{d}t}\Big(\frac{\mathrm{d}x(t)}{\mathrm{d}t}-u(t)\Big)+c(t)\frac{\mathrm{d}x(t)}{\mathrm{d}t}+k(t)x(t)=F(t), \tag{1}$$

where $x(t)$, $c(t)$, and $k(t)$ denote the displacement, damping, and stiffness, respectively; $u(t)$ represents the velocity of the mass element $\mathrm{d}m$ separated from the system.

A representative engineering realization of such systems is the liquid-propellant rocket shown in Fig. 2(a), where the continuous expulsion of high-velocity gases induces irreversible mass depletion. However, the present study does not model the main propulsion dynamics driven by this exhaust; instead, it focuses on the internal structural vibrations (e.g., payload isolation) induced by mass consumption[7]. In this specific context, the separating mass (fuel/oxidizer) is assumed to retain the instantaneous velocity of the local primary system relative to the inertial frame, implying $u(t)=\frac{\mathrm{d}x(t)}{\mathrm{d}t}$. As established by Eke and Mao[2], this zero-relative-velocity condition inherently eliminates the time-dependent thrust effect, allowing the model to focus on the transient dynamic response rather than the macroscopic propulsion path. Under this assumption, the reactive force term in Eq. (1) vanishes, simplifying the governing equation to a form that is formally analogous to a constant-mass oscillator, while the time-varying mass remains encapsulated in the inertial term[61]:

$$m(t)\frac{\mathrm{d}^2x(t)}{\mathrm{d}t^2}+c\frac{\mathrm{d}x(t)}{\mathrm{d}t}+kx(t)=F(t). \tag{2}$$

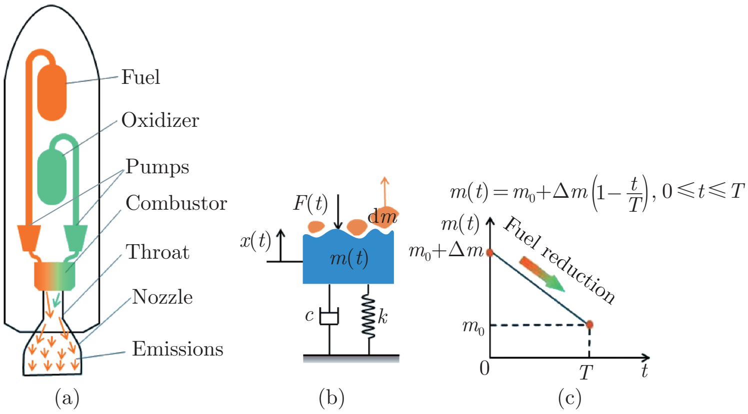

Fig. 2 Schematic representation of the rocket system: (a) structural components of a liquid rocket; (b) simplified vibration isolation model of the rocket system; (c) functional representation of the fuel-mass reduction profile (color online)

By assuming a linear fuel consumption profile, as illustrated in Fig. 2(c), the time-dependent mass $m(t)$ of the system is described by

$$m(t) = m_0 + \Delta m\Big(1 - \frac{t}{T}\Big), \quad 0 \leqslant t \leqslant T, \tag{3}$$

where m_0 and Δm denote the mass of the fuel tank and the initial fuel mass at liftoff, respectively. The variable T represents the combustion duration until the fuel is fully consumed. To streamline the analysis, the vibration induced by the propellant slosh and operation of auxiliary electronic equipment is modeled as a sinusoidal excitation. This motion induces a vertical sinusoidal force within the fuel tank. Subsequently, substituting Eq. (3) into Eq. (2) yields the differential equation for the coupled payload-isolation system,

$$\Big(m_0 + \Delta m\Big(1 - \frac{t}{T}\Big)\Big)\frac{\mathrm{d}^2 x}{\mathrm{d}t^2} + c\frac{\mathrm{d}x}{\mathrm{d}t} + kx = F_0 \sin(\omega t), \tag{4}$$

where F_0 denotes the amplitude of the excitation force arising from fuel sloshing as well as the dynamic loads generated during the operation of auxiliary mechanical subsystems. To derive a tractable formulation for mass-varying systems, a mass parameter ε is defined as

$$\varepsilon = m_0 + \Delta m(1 - t/T). \tag{5}$$

To reformulate the displacement-time dependence, the response derivative $\frac{\mathrm{d}x}{\mathrm{d}t}$ is recast in terms of ε, yielding

$$\frac{\mathrm{d}x}{\mathrm{d}t} = \frac{\mathrm{d}x}{\mathrm{d}\varepsilon}\cdot\frac{\mathrm{d}\varepsilon}{\mathrm{d}t} = -\frac{\Delta m}{T}\frac{\mathrm{d}x}{\mathrm{d}\varepsilon}, \tag{6}$$

$$\frac{\mathrm{d}^2 x}{\mathrm{d}t^2} = \Big(\frac{\Delta m}{T}\Big)^2\frac{\mathrm{d}^2 x}{\mathrm{d}\varepsilon^2}. \tag{7}$$

The time t is further represented by ε as

$$t = T\Big(1 - \frac{\varepsilon - m_0}{\Delta m}\Big). \tag{8}$$

Therefore, Eq. (5) can be recast into

$$\Big(\frac{\Delta m}{T}\Big)^2\varepsilon\frac{\mathrm{d}^2 x}{\mathrm{d}\varepsilon^2} - c\frac{\Delta m}{T}\frac{\mathrm{d}x}{\mathrm{d}\varepsilon} + kx = F\Big(T\Big(1 - \frac{\varepsilon - m_0}{\Delta m}\Big)\Big). \tag{9}$$

The solution to the above equation comprises two elements: the general solution to the corresponding homogeneous differential equation and the particular solution to the equation itself. However, deriving general solutions for time-varying mass systems poses a fundamentally greater challenge than for constant-mass systems. In fact, analytical solutions for the vast majority of such systems remain intractable. Therefore, developing a tactical means to obtain analytical solutions is of paramount importance for the accurate assessment of vibration control performance in time-varying mass systems.

3 Transform-based solutions

Pursuing analytical solutions for time-varying mass systems often involves transforming the governing equations into established canonical forms. The Bessel functions are particularly relevant in this context. As canonical solutions to the Bessel differential equation, they form a complete orthogonal set and are renowned for describing wave phenomena and oscillatory behaviors, even in problems that are not intrinsically defined in cylindrical or spherical geometries. This versatility suggests that through an appropriate variable transformation, the equations of certain time-varying mass systems might be recast into the Bessel equation. Successfully doing so is highly advantageous, granting direct access to well-established properties and asymptotic behaviors. Consequently, this approach not only yields a closed-form analytical solution but also provides profound physical insight into its dynamic characteristics, thereby enabling a more rigorous assessment of its vibration control performance.

3.1 Transformation to canonical Bessel form

For reference, the standard Bessel equation is given by

$$t^2\frac{\mathrm{d}^2y}{\mathrm{d}t^2}+t\frac{\mathrm{d}y}{\mathrm{d}t}+(t^2-v^2)y=0. \tag{10}$$

First, two parameters w and τ are introduced, whose expressions are given by the product of the independent variable x and a polynomial in ε, and the product of χ and a polynomial in ε, respectively, i.e.,

$$\begin{cases} w=\varepsilon^p x, \\ \tau=\chi\varepsilon^q, \end{cases} \to \begin{cases} x(t)=\varepsilon^{-p}w, \\ \dfrac{\mathrm{d}\tau}{\mathrm{d}\varepsilon}=q\chi\varepsilon^{q-1}. \end{cases} \tag{11}$$

Here, p, q, and χ are unknown parameters.

According to Eq. (11), one has

$$\frac{\mathrm{d}x}{\mathrm{d}\varepsilon}=-p\varepsilon^{-p-1}w+q\chi\varepsilon^{q-p-1}\frac{\mathrm{d}w}{\mathrm{d}\tau}, \tag{12}$$

$$\frac{\mathrm{d}^2x}{\mathrm{d}\varepsilon^2}=p(p+1)\varepsilon^{-p-2}w+(\chi q(q-p-1)-pq\chi)\varepsilon^{q-p-2}\frac{\mathrm{d}w}{\mathrm{d}\tau}+q^2\chi^2\varepsilon^{2q-p-2}\frac{\mathrm{d}^2w}{\mathrm{d}\tau^2}. \tag{13}$$

Substituting Eqs. (12) and (13) into the corresponding homogeneous differential equation gives

$$\begin{aligned}&\Big(\frac{\Delta m}{T}\Big)^2q^2\chi^2\varepsilon^{2q-p-1}\frac{\mathrm{d}^2w}{\mathrm{d}\tau^2}+\Big(\Big(\frac{\Delta m}{T}\Big)^2(\chi q(q-2p-1))-c\frac{\Delta m}{T}q\chi\Big)\varepsilon^{q-p-1}\frac{\mathrm{d}w}{\mathrm{d}\tau}\\&+\Big(\Big(\frac{\Delta m}{T}\Big)^2p(p+1)\varepsilon^{-p-1}+c\frac{\Delta m}{T}p\varepsilon^{-p-1}+k\varepsilon^{-p}\Big)w=0.\end{aligned} \tag{14}$$

A comparison between Eq. (14) and the standard Bessel equation reveals that the coefficient preceding the second-order derivative in Eq. (14) differs by a factor of $(\Delta m/T)^{-2}q^{-2}\varepsilon^{p+1}$. To transform Eq. (14) into the standard Bessel form, both sides of the equation are multiplied by $(\Delta m/T)^{-2}q^{-2}\varepsilon^{p+1}$, yielding

$$\begin{aligned}&\chi^2\varepsilon^{2q}\frac{\mathrm{d}^2w}{\mathrm{d}\tau^2}+\Big((q-2p-1)-c\Big(\frac{\Delta m}{T}\Big)^{-1}\Big)q^{-1}\chi\varepsilon^q\frac{\mathrm{d}w}{\mathrm{d}\tau}\\&+\Big(\frac{\Delta m}{T}\Big)^{-2}q^{-2}\Big(\Big(\frac{\Delta m}{T}\Big)^2p(p+1)+c\frac{\Delta m}{T}p+k\varepsilon\Big)w=0.\end{aligned}\tag{15}$$

Comparing Eq. (15) with the standard Bessel equation yields

$$\frac{Tk}{\Delta mq^2}=\chi^2,\quad \Big((q^{-1}(q-2p-1))-\Big(\frac{T}{\Delta m}\Big)cq^{-1}\Big)=1,\quad 2q=1.\tag{16}$$

According to Eq. (16), the three unknown parameters in Eq. (11) can be determined as

$$q=\frac{1}{2},\quad \chi=\frac{2T\sqrt{k}}{\Delta m},\quad p=-\frac{cT}{2\Delta m}-\frac{1}{2}.\tag{17}$$

Substituting Eq. (17) into Eq. (11) allows the newly introduced parameters to be redefined as

$$w=\varepsilon^{-\frac{1}{2}\left(\frac{cT}{\Delta m}+1\right)}x(t),\tag{18}$$

$$\tau=\frac{2T\sqrt{k\varepsilon}}{\Delta m}.\tag{19}$$

Then, the original displacement response x and the derivation of τ with respect to ε can be reformulated as

$$x(t)=\varepsilon^{\frac{1}{2}\left(\frac{cT}{\Delta m}+1\right)}w,\quad \frac{\mathrm{d}\tau}{\mathrm{d}\varepsilon}=\frac{T\sqrt{k}}{\Delta m}\varepsilon^{-\frac{1}{2}}.\tag{20}$$

Substituting Eq. (20) into Eq. (12) gives

$$\frac{\mathrm{d}x}{\mathrm{d}\varepsilon}=\Big(\frac{cT}{2\Delta m}+\frac{1}{2}\Big)\varepsilon^{\frac{cT}{2\Delta m}-\frac{1}{2}}w+\frac{T\sqrt{k}}{\Delta m}\varepsilon^{\frac{cT}{2\Delta m}}\frac{\mathrm{d}w}{\mathrm{d}\tau}.\tag{21}$$

Differentiating Eq. (21) once more with respect to the variable ε yields

$$\begin{aligned}\frac{\mathrm{d}^2x}{\mathrm{d}\varepsilon^2}&=\Big(-\frac{cT}{2\Delta m}-\frac{1}{2}\Big)\Big(-\frac{cT}{2\Delta m}+\frac{1}{2}\Big)\varepsilon^{\frac{cT}{2\Delta m}-\frac{3}{2}}w\\&+\Big(\frac{cT^2\sqrt{k}}{2\Delta m^2}+\Big(\frac{cT}{2\Delta m}+\frac{1}{2}\Big)\frac{T\sqrt{k}}{\Delta m}\Big)\varepsilon^{\frac{cT}{2\Delta m}-1}\frac{\mathrm{d}w}{\mathrm{d}\tau}+\frac{T^2k}{\Delta m}\varepsilon^{\frac{cT}{2\Delta m}-\frac{1}{2}}\frac{\mathrm{d}^2w}{\mathrm{d}\tau^2}.\end{aligned}\tag{22}$$

Substituting Eqs. (21) and (22) into Eq. (9), the differential equation of the rocket fuel consumption system can be reformulated as a second-order nonlinear differential equation in terms of the newly introduced variable w with respect to τ, namely

$$\tau^2\frac{\mathrm{d}^2w}{\mathrm{d}\tau^2}+\tau\frac{\mathrm{d}w}{\mathrm{d}\tau}+\Big(\tau^2-\Big(\frac{cT}{\Delta m}+1\Big)^2\Big)w=\Big(\frac{2T}{\Delta m}\Big)^2\Big(\frac{\Delta m\tau}{2\sqrt{k}T}\Big)^{-\frac{cT}{\Delta m}+1}F\Big(T\Big(1-\frac{\varepsilon-m_0}{\Delta m}\Big)\Big).\tag{23}$$

A comparison between the above expression and the standard Bessel equation indicates that the equation of motion for the time-varying mass system is rigorously mapped into a Bessel form with an excitation term. Physically, the transformed independent variable τ serves as an effective time scaling that normalizes the dynamics of the system. As mass depletion reduces the system inertia, the instantaneous natural frequency continuously increases. This variable dynamically scales the physical time axis to accommodate this accelerating dynamic rhythm, thereby intrinsically capturing the evolving dynamic characteristics and mapping the non-stationary physical process into a normalized mathematical space.

3.2 General and particular solutions

The solution to Eq. (23) needs to be obtained to predict the dynamic response of the tank by reversing the sequence of parameter transformations. Similarly, the solution should consist of the general solution to the corresponding homogeneous equation plus the particular solution induced by the excitation term. The procedure is described below.

3.2.1 General solution

The order υ serves as the fingerprint of the Bessel equation, uniquely determining the characteristics of its solutions, which is given by

$$\upsilon = \frac{cT}{\Delta m} + 1. \tag{24}$$

Equation (23) can be rewritten as

$$\tau^2 \frac{\mathrm{d}^2 w}{\mathrm{d}t^2} + \tau \frac{\mathrm{d}w}{\mathrm{d}t} + (\tau^2 - \upsilon^2) w = \Big(\frac{2T}{\Delta m}\Big)^2 \Big(\frac{\Delta m \tau}{2\sqrt{k}T}\Big)^{-\frac{cT}{\Delta m}+1} F\Big(T\Big(1 - \frac{\varepsilon - m_0}{\Delta m}\Big)\Big). \tag{25}$$

As well-established, a homogeneous equation corresponding to Eq. (25) constitutes a standard Bessel equation of the order υ. The general solution therefore comprises the Bessel functions of the first and second kinds, $\mathrm{J}_\upsilon(z)$ and $\mathrm{Y}_\upsilon(z)$, which are defined as

$$\mathrm{Y}_\upsilon(z) = \frac{J_\upsilon(z)\cos(\upsilon\pi) - J_{-\upsilon}(z)}{\sin(\upsilon\pi)}, \tag{26}$$

$$\mathrm{J}_\upsilon(z) = \sum_{m=1}^{\infty} \frac{(-1)^m}{m!\Gamma(\upsilon + m + 1)} \Big(\frac{z}{2}\Big)^{2m+\upsilon}. \tag{27}$$

$\mathrm{J}_\upsilon(z)$ and $\mathrm{Y}_\upsilon(z)$ are linearly independent solutions to the Bessel equation. Therefore, the general solution can be expressed as

$$y_q(z) = C_1 \mathrm{J}_\upsilon(z) + C_2 \mathrm{Y}_\upsilon(z), \tag{28}$$

where the constants C_1 and C_2 are determined by initial conditions.

3.2.2 Method of variation of parameters

For the present system, determining the particular solutions under excitation is challenging. The method of variation of parameters provides a viable pathway for this task.

Consider the following inhomogeneous Bessel equation:

$$z^2 \frac{\mathrm{d}^2 y}{\mathrm{d}z^2} + z \frac{\mathrm{d}y}{\mathrm{d}z} + (z^2 - \upsilon^2) y = f(z). \tag{29}$$

Let $y_1(z)$ and $y_2(z)$ be the two known, linearly independent solutions of the homogeneous form of Eq. (29). In the context of the Bessel equation analyzed in the preceding section, these correspond directly to the Bessel functions of the first and second kinds, $\mathrm{J}_\upsilon(z)$ and $\mathrm{Y}_\upsilon(z)$, respectively. According to the method of variation of parameters, the complementary function can be expressed as

$$y_{\mathrm{p}}(z) = C_1 y_1(z) + C_2 y_2(z). \tag{30}$$

The basic idea of the method of variation of parameters is to replace the constants C_1 and C_2 with the unknown functions $u_1(z)$ and $u_2(z)$. Accordingly, the complementary function becomes

$$y_{\mathrm{p}}(z) = u_1(z) y_1(z) + u_2(z) y_2(z). \tag{31}$$

To determine $u_1(z)$ and $u_2(z)$, both sides of Eq. (31) are first differentiated with respect to z, yielding

$$y_{\mathrm{p}}'(z) = u_1(z)y_1'(z) + u_2(z)y_2'(z) + u_1'(z)y_1(z) + u_2'(z)y_2(z). \tag{32}$$

A key assumption is adopted to simplify the problem and guarantee a unique solution,

$$u_1'(z)y_1(z) + u_2'(z)y_2(z) = 0. \tag{33}$$

Accordingly, Eq. (33) takes the form of

$$y_{\mathrm{p}}'(z) = u_1'(z)y_1(z) + u_2'(z)y_2(z). \tag{34}$$

Performing a second differentiation on Eq. (34) with respect to z gives

$$y_{\mathrm{p}}''(z) = u_1(z)y_1''(z) + u_2(z)y_2''(z) + u_1'(z)y_1'(z) + u_2'(z)y_2'(z). \tag{35}$$

Substituting Eqs. (32), (31), and (35) into the inhomogeneous Bessel equation leads to

$$\sum_{k=1}^{2} u_k(z)(z^2 y_k''(z) + z y_k'(z) + (z^2 - \upsilon^2)y_k(z)) + z^2 \sum_{l=1}^{2} u_l'(z)y_l'(z) = f(z). \tag{36}$$

Since $y_1(z)$ and $y_2(z)$ satisfy the homogeneous equation, the first term in Eq. (36) is identically zero. Consequently, Eq. (36) is reduced to

$$u_1'(z)y_1'(z) + u_2'(z)y_2'(z) = \frac{f(z)}{z^2}, \tag{37}$$

in which $u_1'(z)$ and $u_2'(z)$ are governed by a linear system comprising Eqs. (33) and (37), whose solutions write

$$u_1'(z) = \frac{-y_2(z)f(z)}{z^2(y_1y_2' - y_1'y_2)}, \quad u_2'(z) = \frac{y_1(z)f(z)}{z^2(y_1y_2' - y_1'y_2)}. \tag{38}$$

Upon integration, one has

$$u_1(z) = \int \frac{y_2(z)f(z)}{z^2(y_1y_2' - y_1'y_2)}\mathrm{d}z, \quad u_2(z) = \int \frac{y_1(z)f(z)}{z^2(y_1y_2' - y_1'y_2)}\mathrm{d}z. \tag{39}$$

The particular solution to the Bessel equation with an excitation term is thus derived by substituting Eq. (39) into Eq. (31), resulting in

$$y_{\mathrm{p}}(z) = -y_1(z)\int \frac{y_2(z)f(z)}{z^2(y_1y_2' - y_1'y_2)}\mathrm{d}z + y_2(z)\int \frac{y_1(z)f(z)}{z^2(y_1y_2' - y_1'y_2)}\mathrm{d}z. \tag{40}$$

Evidently, the method of variation of parameters provides a pivotal avenue for deriving a closed-form solution to Bessel-type equations with excitation terms. This approach offers an ideal framework for analyzing the dynamic behavior of time-varying mass systems and evaluating the efficacy of vibration control strategies.

3.3 Closed-form solution

By applying the method of variation of parameters, the general solution to the Bessel equation with an excitation term can be expressed explicitly as the sum of the complementary solution (corresponding to the homogeneous equation) and a particular solution driven by the excitation, formulated as follows:

$$w(\tau) = C_1y_1(\tau) + C_2y_2(\tau) - y_1(\tau)\int \frac{y_2(\tau)f(\tau)}{\tau^2(y_1(\tau)y_2(\tau)' - y_1(\tau)'y_2(\tau))}\mathrm{d}\tau$$

$$+ y_2(\tau)\int \frac{y_1(\tau)f(\tau)}{\tau^2(y_1(\tau)y_2(\tau)' - y_1(\tau)'y_2(\tau))}\mathrm{d}\tau, \tag{41}$$

where

$$y_1(\tau) = \mathrm{J}_\upsilon(\tau) = \sum_{m=1}^{\infty}\frac{(-1)^m}{m!\Gamma(\upsilon+m+1)}\Big(\frac{\tau}{2}\Big)^{2m+\upsilon}\upsilon = \frac{cT}{\Delta m}+1, \tag{42}$$

$$y_2(\tau) = \mathrm{Y}_\upsilon(\tau) = \frac{\mathrm{J}_\upsilon(\tau)\cos(\upsilon\pi) - \mathrm{J}_{-\upsilon}(\tau)}{\sin(\upsilon\pi)}\upsilon = \frac{cT}{\Delta m}+1, \tag{43}$$

$$f(\tau) = \Big(\frac{2T}{\Delta m}\Big)^2\Big(\frac{\Delta m\tau}{2T}\Big)^{-\frac{cT}{\Delta m}+1}\sin\Big(T\Big(1-\frac{\frac{\tau^2}{k}\big(\frac{\Delta m}{2T}\big)^2 - m_0}{\Delta m}\Big)\Big). \tag{44}$$

By applying the parametric transformation given in Eq. (20), $x(t)$ can be derived in terms of the parameter ε as

$$x(t) = \varepsilon^{\frac{1}{2}\left(\frac{cT}{\Delta m}+1\right)}w\Big(\frac{2T\sqrt{k\varepsilon}}{\Delta m}\Big), \tag{45}$$

where $w(2T\sqrt{k\varepsilon}/\Delta m)$ can be calculated using Eq. (41).

Although Eq. (45) defines the relationship between x and w, w itself remains a function of ε. Consequently, substituting an explicit expression $\varepsilon = m_0 + \Delta m(1-t/T)$ into Eq. (45) yields the full time-domain solution $x(t)$, thereby describing the temporal evolution of the displacement response in the time-varying mass system, namely

$$x(t) = \Big(m_0 + \Delta m\Big(1-\frac{t}{T}\Big)\Big)^{\frac{1}{2}\left(\frac{cT}{\Delta m}+1\right)}w\Big(\frac{2T\sqrt{k\big(m_0+\Delta m\big(1-\frac{t}{T}\big)\big)}}{\Delta m}\Big). \tag{46}$$

A challenge in the theoretical process of visualizing the closed-form solution to the original equation of motion is the introduction of an indefinite integral by the method of variation of parameters. Simplifying the product function reveals that this indefinite integral can neither be derived from the original function nor be expressed in terms of elementary functions. For the two classes of Bessel equations under consideration, both represent solutions expressed in terms of homogeneous Bessel functions; in other words, they satisfy

$$\tau^2\mathrm{J}_\upsilon''(\tau) + \tau\mathrm{J}_\upsilon'(\tau) + (\tau^2 - u^2)\mathrm{J}_\upsilon(\tau) = 0, \tag{47}$$

$$\tau^2\mathrm{Y}_\upsilon''(\tau) + \tau\mathrm{Y}_\upsilon'(\tau) + (\tau^2 - u^2)\mathrm{Y}_\upsilon(\tau) = 0. \tag{48}$$

The Wronskian determinant of the Bessel functions, defined as follows, serves as a standard tool for verifying their linear independence and elucidating the subsequent relationships:

$$G(\tau) = \mathrm{J}_\upsilon(\tau)\mathrm{Y}_\upsilon'(\tau) - \mathrm{J}_\upsilon'(\tau)\mathrm{Y}_\upsilon(\tau). \tag{49}$$

Differentiating the above expression with respect to τ yields

$$G'(\tau) = \mathrm{J}_\upsilon(\tau)\mathrm{Y}_\upsilon''(\tau) - \mathrm{J}_\upsilon''(\tau)\mathrm{Y}_\upsilon(\tau). \tag{50}$$

From Eqs. (47) and (48), the following relationship can be derived:

$$\mathrm{J}_\upsilon(\tau)\mathrm{Y}_\upsilon''(\tau) = -\mathrm{J}_\upsilon(\tau)\Big(\frac{\tau\mathrm{Y}_\upsilon'(\tau) + (\tau^2-u^2)\mathrm{Y}_\upsilon(\tau)}{\tau^2}\Big), \tag{51}$$

$$\mathrm{J}_\upsilon''(\tau)\mathrm{Y}_\upsilon(\tau) = -\mathrm{Y}_\upsilon(\tau)\Big(\frac{\tau\mathrm{J}_\upsilon'(\tau) + (\tau^2-u^2)\mathrm{J}_\upsilon(\tau)}{\tau^2}\Big). \tag{52}$$

Substituting Eqs. (51) and (52) into Eq. (50) yields $G'(\tau) = \frac{\mathrm{d}G(\tau)}{\mathrm{d}\tau} = -\frac{G(\tau)}{\tau}$.

Since the governing equation is a first-order ordinary differential equation with an intrinsically separable form, it admits a direct solution via the method of separation of variables, expressed as $G(\tau) = \pm \mathrm{e}^{C_3}/\tau$.

Evidently, the coefficient e^{C_3} represents an unknown constant, which is an arbitrary constant dependent on C_3. For simplicity, it can be denoted simply as C_4, allowing the solution for G to be written as $G(\tau) = C_4/\tau$.

The final determination of the coefficient C_4 hinges upon the Wronskian determinant $G(\tau)$, itself defined by the asymptotic expansion of the Bessel function. It is therefore imperative that the preceding derivation serves to procure an analytic form of $G(\tau)$ and to verify that it does not vanish anywhere within the solution interval: a condition that secures the existence of two linearly independent solutions.

As $t \to +\infty$, the Bessel function admits the asymptotic expansion,

$$\mathrm{J}_{\upsilon}(\tau) \sim \frac{1}{\sqrt{2\pi\tau}}\cos\Big(\tau - \frac{\upsilon\pi}{2}\Big), \quad \mathrm{Y}_{\upsilon}(\tau) \sim \frac{1}{\sqrt{2\pi\tau}}\sin\Big(\tau - \frac{\upsilon\pi}{2}\Big). \tag{53}$$

In this case, the Wronskian determinant of the Bessel function is $G(\tau) = 2/(\pi\tau)$.

The persistence of a nonzero Wronskian determinant $G(\tau)$ throughout the solution interval ensures the linear independence of the two solutions. Applying this result to Eq. (50) leads to the determination C_4=$2/\pi$.

The Wronskian determinant $G(\tau) = 2/(\pi\tau)$ is employed to simplify the complex indefinite integrals arising from the parametric calculus of variations, as given by Eq. (41). The latter is simplified as follows:

$$w(\tau) = C_1 y_1(\tau) + C_2 y_2(\tau) - y_1(\tau)\int \frac{\pi y_2(\tau) f(\tau)}{2\tau}\mathrm{d}\tau + y_2(\tau)\int \frac{\pi y_1(\tau) f(\tau)}{2\tau}\mathrm{d}\tau. \tag{54}$$

Clearly, for a given excitation function, the evolution of w with respect to τ can be obtained from Eq. (54). Subsequently, by applying the method of variation of parameters, the evolution of the dynamic response x with respect to time t can be determined.

3.4 Verification

After transforming the equation of motion into a non-homogeneous Bessel equation via the method of variation of parameters, a closed-form solution for the dynamic response of the time-varying mass system has been derived. This solution provides a foundation for evaluating the isolation performance of the vibration isolator. It is imperative, however, that the validity of this closed-form solution be rigorously established prior to its deployment for performance assessment.

3.4.1 Transformation of initial conditions

When solving a Bessel-type equation with an external excitation, the closed-form solution inherently contains unknown coefficients that are intrinsically coupled to the initial conditions of the Bessel functions. However, in time-varying systems governed by fuel combustion dynamics, the initial physical conditions diverge from those of the canonical Bessel formulation. Consequently, a consistent parameter transformation, identical to that employed in reducing the equation of motion to the standard Bessel form, must be implemented to properly map the initial physical conditions onto their Bessel-equation counterparts.

In rocket-launch dynamics, the equations of motion are initialized with zero displacement and zero velocity at $t = 0$. Accordingly, the initial conditions for the second-order differential equation, Eq. (4), write

$$x(0) = 0, \quad x'(0) = 0. \tag{55}$$

Substitution of Eq. (55) into Eq. (5) yields

$$\begin{pmatrix} x(\varepsilon) \\ x'(\varepsilon) \end{pmatrix}\Bigg|_{\varepsilon=m_0+\Delta m} = \begin{pmatrix} 0 \\ 0 \end{pmatrix}. \tag{56}$$

The value of the third transformed variable τ follows from the substitution of Eq. (56) into Eqs. (18) and (19) as $\tau = 2T\sqrt{k(m_0+\Delta m)}/\Delta m$.

According to Eq. (21), the equality holds only when $w(\tau) = 0$ and $\frac{\mathrm{d}w}{\mathrm{d}\tau} = 0$. Under these conditions, the initial values for the third transformed differential equation (25) are specified by

$$\begin{pmatrix} w(\tau) \\ w'(\tau) \end{pmatrix}\Bigg|_{\tau=\frac{2T\sqrt{k(m_0+\Delta m)}}{\Delta m}} = \begin{pmatrix} 0 \\ 0 \end{pmatrix}. \tag{57}$$

Based on the previously established initial conditions for the third differential equation, the corresponding analytical solution is solved, illustrating the mapping from w to τ. Applying the inverse parametric transformation in Eq. (20) yields the mapping from x to ε. Subsequently, by employing the inverse transformation of Eq. (5), the time-dependent response $x(t)$ can be obtained and presented graphically.

3.4.2 Variable upper-limit integration

In the analysis of time-varying vibration isolation systems, the product function $f(\tau)$ in Eq. (54) contains non-elementary terms such as Bessel functions, whose antiderivative cannot be expressed in a closed form. Conventional indefinite integration, which yields a family of curves $F(\tau)+C$ differing by an arbitrary constant C, is unsuitable for uniquely determining vibration transmittance. To address this limitation, we employ a definite integral with a variable upper limit, given by $F(\xi) = \int_a^\tau f(\xi)\mathrm{d}\xi$, in which a denotes a fixed lower bound. If $f(\tau)$ is continuous, the resulting function represents a single, determinate antiderivative curve, eliminating the ambiguity introduced by the arbitrary constant. Therefore, the continuity of $f(\tau)$ is essential for applying the variable upper-limit integration method. In the aforementioned transformed inhomogeneous Bessel equation, the time domain $(0, T)$ associated with the time-varying process is transformed into $\left(\frac{2T\sqrt{k(m_0+\Delta m)}}{\Delta m}, \frac{2T\sqrt{km_0}}{\Delta m}\right)$.

Because the Bessel functions involved are continuous over this interval, the resulting composite functions given by the following two equations are likewise continuous, thereby satisfying the prerequisite for the variable upper-limit integration method:

$$P(\tau) = \frac{\pi}{2\tau}y_2(\tau)f(\tau) = \frac{\pi}{2\tau}\mathrm{Y}_\upsilon(\tau)\Big(\frac{2T}{\Delta m}\Big)^2\Big(\frac{\Delta m\tau}{2T}\Big)^{-\frac{cT}{\Delta m}+1}\sin\Bigg(T\Bigg(1-\frac{\frac{\tau^2}{k}\big(\frac{\Delta m}{2T}\big)^2 - m_0}{\Delta m}\Bigg)\Bigg), \tag{58}$$

$$Q(\tau) = \frac{\pi}{2\tau}y_1(\tau)f(\tau) = \frac{\pi}{2\tau}\mathrm{J}_\upsilon(\tau)\Big(\frac{2T}{\Delta m}\Big)^2\Big(\frac{\Delta m\tau}{2T}\Big)^{-\frac{cT}{\Delta m}+1}\sin\Bigg(T\Bigg(1-\frac{\frac{\tau^2}{k}\big(\frac{\Delta m}{2T}\big)^2 - m_0}{\Delta m}\Bigg)\Bigg). \tag{59}$$

The numerical implementation of the analytical solution $w(\tau)$ is carried out in three sequential stages. First, the coefficients C_1 and C_2 in Eq. (54) are obtained by solving the linear system arising from the initial conditions specified in Eq. (57). These coefficients fully determine the homogeneous component of the solution. Next, the integral term in the particular solution, for which no closed-form antiderivative exists, is evaluated numerically as a definite integral with a variable upper limit, ensuring that the additive-constant ambiguity inherent in indefinite integration is avoided. Finally, a cumulative-integral interpolation method is used to efficiently reconstruct a high-accuracy, continuous representation of $w(\tau)$ over a dense grid spanning the solution interval.

Using the parameters in Table 1 and following the solution procedure outlined above, the variation in w with respect to τ is obtained, as shown in Fig. 3(a). In the first stage of parametric transformation, this result is mapped to the intermediate variable ε, yielding the variation in x with respect to ε, as illustrated in Fig. 3(b). In the subsequent stage, an additional transformation from ε to physical time t is performed, producing the temporal evolution of the displacement response of the fuel tank, which is presented in Fig. 3(c). These sequential transformations establish a complete correspondence between the solution in the auxiliary domain and the physical displacement-time characteristics of the original system.

Table 1 The system parameters used for calculations

Parameter	Symbol	Value	Parameter	Symbol	Value
Constant mass	m_0	5 kg	Damping coefficient	c	2 N·s/m
Time-dependent mass	Δm	50 kg	Stiffness	K	10 000 N/m
Combustion duration	T	25 s			

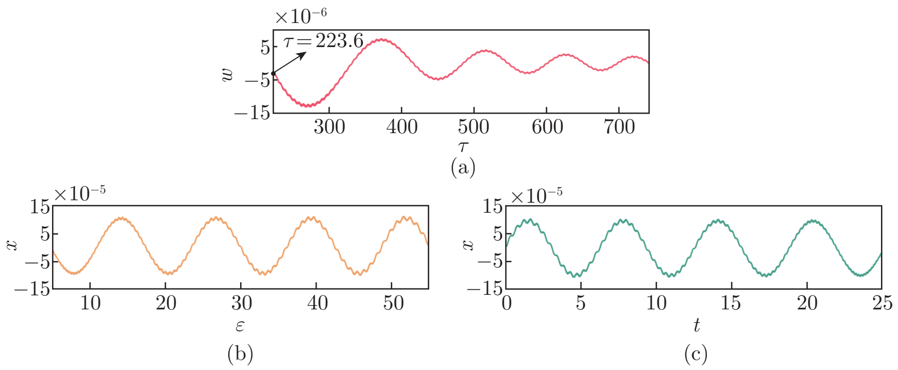

Fig. 3 Solutions to the three differential equations involved in the inverse transformation at an excitation frequency of 0.16 Hz: (a) variation in w with respect to τ; (b) displacement x as a function of intermediate variable ε; (c) displacement x as a function of time t (color online)

For the excited Bessel function, the amplitude of $w(\tau)$ decays markedly as τ increases. After mapping to the intermediate variable ε, the amplitude modulation of $x(\varepsilon)$ is substantially attenuated relative to $w(\tau)$. A further transformation to physical time t shows that the envelope of $x(t)$ varies only slowly, indicating a time-varying system with gradually evolving parameters. Despite the differing amplitude envelopes across the three representations, the responses share the same oscillation frequency. Moreover, successive responses exhibit an approximately $\pi/2$ phase shift relative to their predecessors. These observations confirm that the closed-form expressions obtained via parametric transformations can capture the dynamic response of a time-varying mass system induced by fuel consumption, thereby providing a sound basis for rapid evaluation of vibration isolation performance.

3.4.3 Effect of the lower limit of integration

The selection of the lower limit of integration a in the variable upper-limit integral constitutes a critical yet often underexplored factor that can directly affect the accuracy of the resulting analytical solution. To investigate the effect of the lower integration limit on the computational results, the parameters listed in Table 1 are used to calculate the displacement responses of the time-varying mass system for various values of a. The corresponding comparisons are shown in Fig. 4.

To further quantify the accuracy of analytical solutions, an absolute error index is defined as $E_{\mathrm{a}} = |x(t)_{\mathrm{n}} - x(t)_{\mathrm{a}}|$, where $x(t)_{\mathrm{n}}$ represents the result obtained with the numerical method, and $x(t)_{\mathrm{a}}$ represents the one obtained with the analytical method. To evaluate the influence of the integration lower limit a on the accuracy of the analytical reconstruction, a comparative analysis is performed against the numerical benchmark response. The numerical benchmark response is obtained with the explicit Runge-Kutta (4, 5) method. To ensure sufficient resolution for

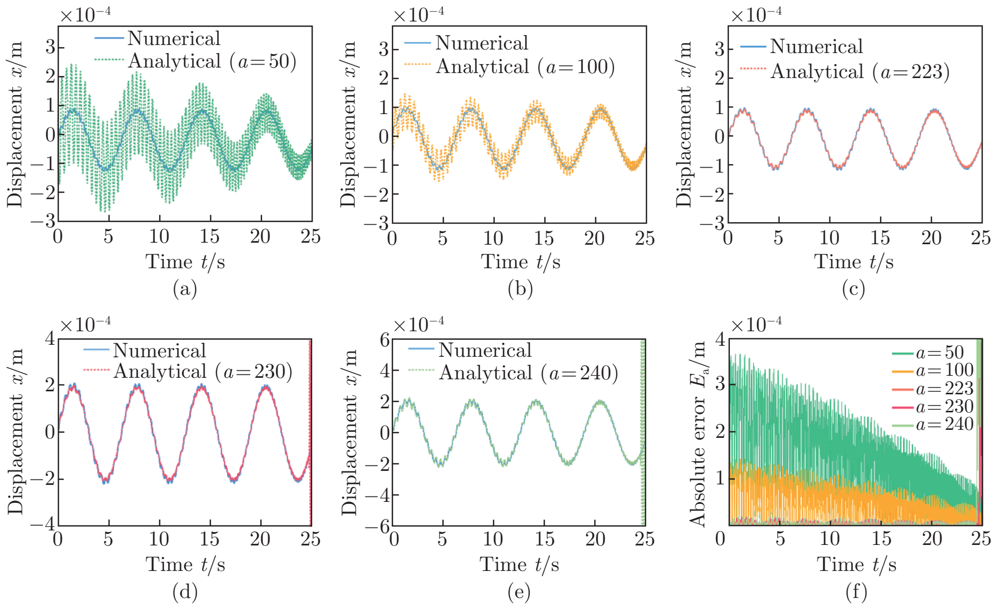

Fig. 4 Comparison of analytical and numerical solutions obtained via the variable upper-limit integration method: (a) $a = 50$, (b) $a = 100$, (c) $a = 223$, (d) $a = 230$, and (e) $a = 240$; (f) absolute errors between analytical and numerical solutions at different a, where the maximum absolute errors are as follows: $E_{\mathrm{a,max}} = 3.65 \times 10^{-4}$ for $a = 50$, $E_{\mathrm{a,max}} = 1.65 \times 10^{-4}$ for $a = 100$, and $E_{\mathrm{a,max}} = 1.5 \times 10^{-5}$ for $a = 223$, 230, 240, and $E_{\mathrm{a,max}}$ is evidently larger than 1.5×10^{-5} (color online)

high-frequency oscillations and guarantee benchmark accuracy, the discrete output time step is set to $\Delta t = 0.01\,\mathrm{s}$, governed by internal integration tolerances (a relative tolerance of 10^{-3} and an absolute tolerance of 10^{-6}). Figures 4(a)–4(c) illustrate the temporal evolutions of displacement $x(t)$ for $a = 50$, 100, 223, respectively, while Fig. 4(f) depicts E_{a} along with their maximum values.

The results demonstrate that the choice of a significantly affects the fidelity of the analytical solution. For $a = 50$, as shown in Fig. 4(a), the analytical solution exhibits pronounced high-frequency oscillations, leading to a substantial deviation from the numerical baseline. This discrepancy is reflected in Fig. 4(f), where the maximum absolute error reaches $3.65 \times 10^{-4}\,\mathrm{m}$. As the limit is increased to $a = 100$ in Fig. 4(b), the error envelope contracts; however, a visible oscillatory discrepancy persists, yielding a maximum error of $1.45 \times 10^{-4}\,\mathrm{m}$. In contrast, when $a = 223$, the analytical curve becomes virtually indistinguishable from the numerical benchmark over the entire time interval, as shown in Fig. 4(c). The maximum absolute error is suppressed to $1.5 \times 10^{-5}\,\mathrm{m}$, which is an order of magnitude lower than that for $a = 50$.

However, as the limit is further increased beyond this point (e.g., $a = 230$ and $a = 240$), the analytical solutions begin to diverge significantly near the end of the time-varying process. Notably, for $a = 240$, this divergence occurs even earlier than that for $a = 230$, and their maximum errors markedly exceed those of the previous configurations. This phenomenon arises because $a \approx 223.6$ corresponds precisely to the theoretical lower boundary ($\tau_{\min}$) of the physically valid domain mapping the combustion endpoint ($t = 25\,\mathrm{s}$). Selecting an integration limit $a > 223.6$ artificially truncates essential physical integration information required to satisfy the dynamic evolution of the system, thereby triggering numerical instability. Altogether, these results reaffirm that the lower limit a is not an innocuous parameter, and the solution accuracy does not monotonically increase with a. Rather, the error follows a U-shaped trend, possessing a a strict physical optimal value, which ensures that the analytical solution perfectly spans the physical boundaries without introducing non-physical artifacts or truncating dynamic information, thereby achieving complete consistency with the numerical benchmark response.

3.4.4 Determination of integration lower bound

Building on the conclusion that the integration lower limit a is critical for solution accuracy, a quantitative framework is established to determine its optimal value. As illustrated in Fig. 5, the root-mean-square error (RMSE) between the analytical and numerical solutions is adopted as the objective function to be minimized. The RMSE, denoted by E_{RMS}, is defined as

$$E_{\mathrm{RMS}} = \sqrt{\frac{1}{N}\sum_{i=1}^{N}(x_{\mathrm{a}}(t_i;a) - x_{\mathrm{n}}(t_i))^2}, \tag{60}$$

where $(t_i)_{i=1}^{N}$ are the sampling instants, $x_{\mathrm{a}}(t,a)$ is the analytical solution parameterized by the lower limit a, and $x_{\mathrm{n}}(t)$ represents the corresponding numerical benchmark.

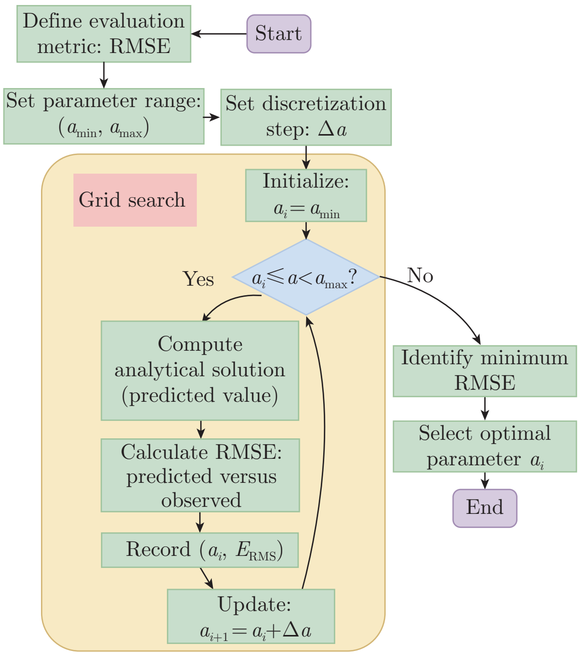

Fig. 5 Flowchart of the grid-search procedure for determining the optimal lower limit (color online)

Optimization is implemented via a grid search. First, the search range $[a_{\min}, a_{\max}]$ for the lower integration limit is specified, together with a discretization step size Δa. The initial value of a is set to $a_{\min}$, and successive candidate values are generated as $a_i = a_{\min} + i\Delta a$, where i increases until $a_{\max}$ is reached. For each candidate a_i, the analytical solution (the predicted value) is computed, and its RMSE relative to the numerical benchmark (observations) is evaluated. The resulting (a_i, E_{RMS}) pairs are recorded for all i. When the search completes, the value of a_i yielding the minimum RMSE is identified as the optimal lower integration limit. This data-driven selection ensures that the resulting analytical solution simultaneously satisfies the governing differential equation and the initial physical conditions, while ensuring the best agreement with the numerical benchmark. This outcome arises because the RMSE metric inherently evaluates both the consistency of the analytical solution with the initial conditions and its fidelity in reproducing the temporal evolution of the displacement response $x(t)$. The procedure depicted in Fig. 5 thus provides a systematic and reproducible approach for determining the most accurate choice of a.

The displacement responses of the time-varying mass system at various excitation frequencies are computed and compared with the corresponding numerical results, as shown in Fig. 6. Methodologically, this study focuses on analyzing the vibration isolation performance of a mass-varying system induced by fuel combustion, without imposing strict constraints on specific rocket parameters. For reference, in a constant-mass system, the natural frequency is uniquely defined. In contrast, for systems undergoing mass depletion, the natural frequency evolves dynamically from its initial value $\omega_0 = \sqrt{K/(m_0+\Delta m)}$ to the final value $\omega_{\mathrm{f}} = \sqrt{K/m_0}$. With the parameters specified in Table 1, the computed instantaneous natural frequency $\omega(t)$ for the examined time-varying mass system lies within $\omega(t) \in (2.15, 7.12)$ Hz, demonstrating a monotonic increase in the stiffness-to-mass ratio as the mass decreases.

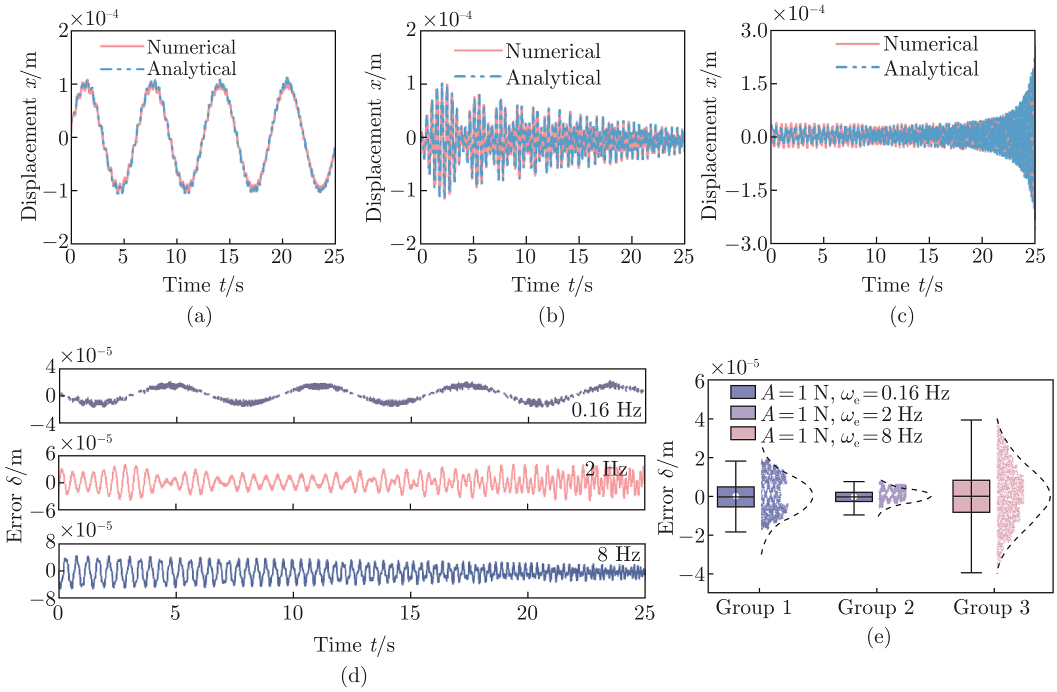

Fig. 6 Comparison of numerical and analytical solutions: (a)–(c) system response diagrams for $f = 0.16$, 2, 8 Hz, respectively; (d) time-domain error plots under three operating conditions; (e) box-and-whisker plots of errors from two methods under three operating conditions (Group 1: 1 N, 0.16 Hz; Group 2: 1 N, 2 Hz; Group 3: 1 N, 8 Hz) (color online)

To verify the accuracy and the robustness of the proposed approach for determining the optimal lower integration limit under distinct dynamic regimes, three representative excitation frequencies are considered, namely 0.16 Hz (sub-resonance), 2 Hz (approaching the initial resonance), and 8 Hz (approaching the final resonance). The excitation amplitude is set to 1 N for all three operating conditions. As illustrated in Figs. 6(a)–6(c), the analytical and numerical displacement responses exhibit nearly identical amplitude and phase variations in all cases, accurately capturing the steady sub-resonant response, transient build-up and decay through resonance, and gradual amplitude growth near resonance. Figure 6(d) displays the time-history of the absolute error between the analytical and numerical solutions for the three excitation frequencies. The error remains consistently small, with minimal fluctuation over time. Figure 6(e) shows the raincloud plots of residual errors, all narrowly distributed around zero with a similar spread across different excitation frequencies, demonstrating the high fidelity and robustness of the proposed analytical approach.

To ensure the completeness of the investigation and further evaluate the performance of the proposed method under different excitation amplitudes, analyses are conducted at a fixed sub-resonant frequency of 0.16 Hz using three excitation amplitude levels, namely 1 N, 2 N, and 3 N. As shown in Fig. 7(a), the analytical and numerical displacement responses exhibit close agreement in both the amplitude and phase across all amplitude levels, accurately capturing the steady-state response characteristics in the sub-resonant regime. Figure 7(b) presents box plots of the error distributions under the three forcing levels, all of which are narrowly clustered around zero with similar spreads, indicating the consistent statistical behavior of the error under varying excitation strengths. Furthermore, Figs. 7(c) and 7(d) show the maximum absolute error and the corresponding RMSE, respectively. Both metrics remain at very low levels and do not increase significantly with increasing excitation amplitudes, further confirming the excellent numerical stability and predictive accuracy of the analytical method across different input magnitudes. In summary, the semi-analytical approach based on variable upper-limit integration is not only applicable to different excitation frequencies but also performs reliably under varying excitation amplitudes, thereby offering a robust and versatile tool for the rapid evaluation of vibration isolation performance in time-varying mass systems.

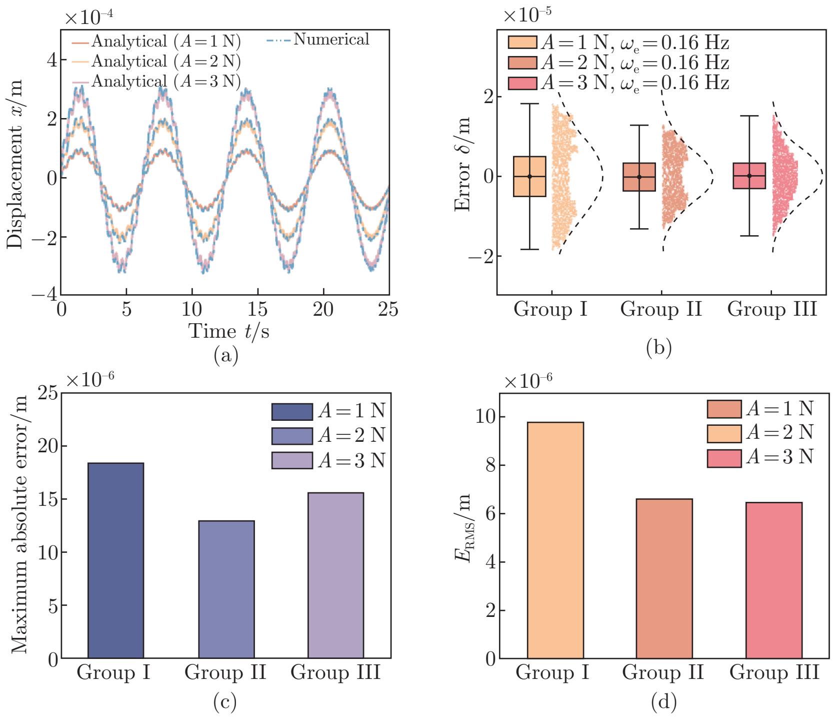

Fig. 7 Comparison of two methods under different excitation amplitudes at 0.16 Hz (Group I: 1 N; Group II: 2 N; Group III: 3 N): (a) system response comparison, (b) error distribution (box plots); (c) maximum absolute error; (d) maximum RMSE (color online)

For vibration scenarios driven by dynamic-force excitations (e.g., fuel sloshing), the isolation performance is commonly assessed in terms of force transmissibility, i.e., the amplitude of the force transmitted to the mounting base. Consequently, an accurate prediction of the forces transmitted through the isolator to the foundation is crucial for evaluating the vibration isolation capability of time-varying mass systems. To reinforce this aspect of the validation, we therefore extend the comparison between the proposed semi-analytical closed-form solution and the numerical reference to the reaction forces, as shown in Figs. 8(a)–8(b). In the figures, "G1-A" and "G1-N" represent the results for Group 1 (0.16 Hz), "G2-A" and "G2-N" represent the results for Group 2 (2 Hz), and "G3-A" and "G3-N" represent the results for Group 3 (8 Hz), where the letters A and N represent the analytical and numerical methods, respectively.

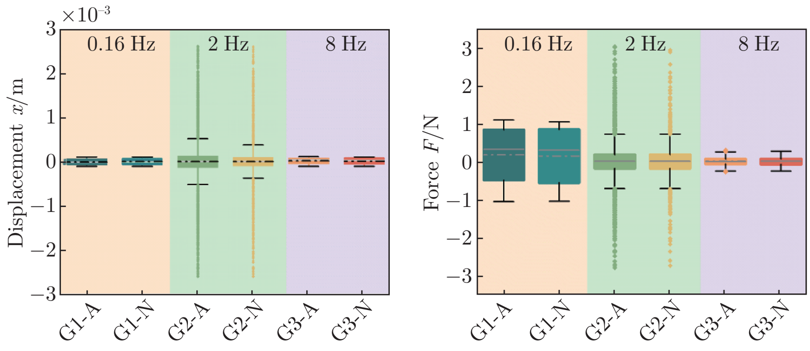

Fig. 8 Box plots of system responses and forces transmitted to the foundation under three operating conditions, determined by both the numerical simulation and the closed-form solution: (a) displacement; (b) transmitted force (color online)

As illustrated in Figs. 8(a)–8(b), box plots are employed to compare the displacement responses and the corresponding reaction forces obtained from the analytical and numerical methods under three representative excitation conditions (0.16 Hz, 2 Hz, and 8 Hz). The nearly overlapping interquartile ranges, medians, and overall distribution spans across all cases indicate that the proposed method not only reproduces the displacement response with high accuracy, but also reliably predicts the transmitted dynamic loads. This consistent agreement in both kinematic and dynamic outputs under sub-resonant, transient-resonant, and near-resonant regimes demonstrates the robustness of the method and its suitability as a reliable analytical tool for force-based vibration isolation evaluation and design.

Furthermore, it is worth noting that although the current derivation and validation focus on single-frequency harmonic excitation, the linearity of the governing equation (2) ensures that the principle of superposition remains strictly valid. By leveraging the Fourier series expansion, any arbitrary periodic external load can be decomposed into a sum of discrete harmonic components. The proposed analytical framework can therefore be systematically extended to obtain the total system response by superimposing the particular solutions corresponding to each harmonic constituent, thereby significantly broadening its engineering applicability.

4 Vibration isolation

Following the development and validation of the closed-form solution in Section 3, this section investigates the transient vibration isolation performance of a time-varying mass system using the proposed methodology. The aim is to derive engineering design implications by exploring the effects of key parameters on force transmission. The study first extends the classical steady-state isolation theory to define a transient performance index, and then analyzes the effects of isolator stiffness and excitation frequency, before formulating the findings as practical design guidelines.

4.1 Vibration isolation evaluation criteria

In classical steady-state analyses, the performance of a vibration isolator is evaluated using the force transmissibility, which becomes effective when the frequency ratio, defined as the ratio of the excitation frequency ω_{e} to the natural frequency ω_{n} of the isolation system, exceeds $\sqrt{2}$. However, systems with time-varying mass fundamentally deviate from this paradigm: during the mass-loss transient, no true steady state exists, as the natural frequency $\omega_{\mathrm{n}}(t)$ evolves continuously over time. This complication necessitates the definition of a transient performance metric. Accordingly, to generalize the energy-based assessment over the entire transient process, the root-mean-square (RMS) force transmissibility is defined as $T_{\mathrm{rms}} = F_{\text{t-rms}}/F_{\text{e-rms}}$, where the RMS values of the transmitted ($F_{\text{t-rms}}$) and excitation ($F_{\text{e-rms}}$) forces are compared.

Although the RMS ratio of instantaneous force responses can partially evaluate the vibration isolation performance of time-varying mass systems, this metric becomes inadequate when the mass variation is of significant intensity, namely, when the response amplitude undergoes pronounced and rapid temporal fluctuations. Under such conditions, reliance on the RMS force ratios alone may yield a biased characterization of the isolation performance. To address this problem, multiple complementary performance metrics are introduced, including time-resolved RMS force ratios evaluated over distinct temporal windows and a failure-time threshold (FTT) that quantifies the loss of isolation effectiveness during periods of pronounced mass variation.

4.2 Results and discussion

The influence of isolator stiffness on the vibration isolation performance is analyzed in Fig. 9. Consistent with the classical theory for constant-mass systems, reducing stiffness generally lowers force transmissibility. However, the time-varying mass introduces a unique dynamic failure mode, quantified here as the FTT.

As shown in Figs. 9(a)–9(c), the continuous depletion of mass causes the instantaneous natural frequency to rise. Consequently, a system that is initially tuned for isolation may drift into the resonance region during operation. For higher stiffness values (e.g., 12 000 N/m and 10 000 N/m), this parameter evolution leads to an FTT event where isolation effectiveness is lost before the mass variation concludes. The RMS analysis in Fig. 9(d) corroborates this, showing that while all configurations are effectively isolated in the initial phase $[0, 1]$ s, the reduced detuning margin in the late phase $[24, 25]$ s triggers resonant amplification for stiffer isolators.

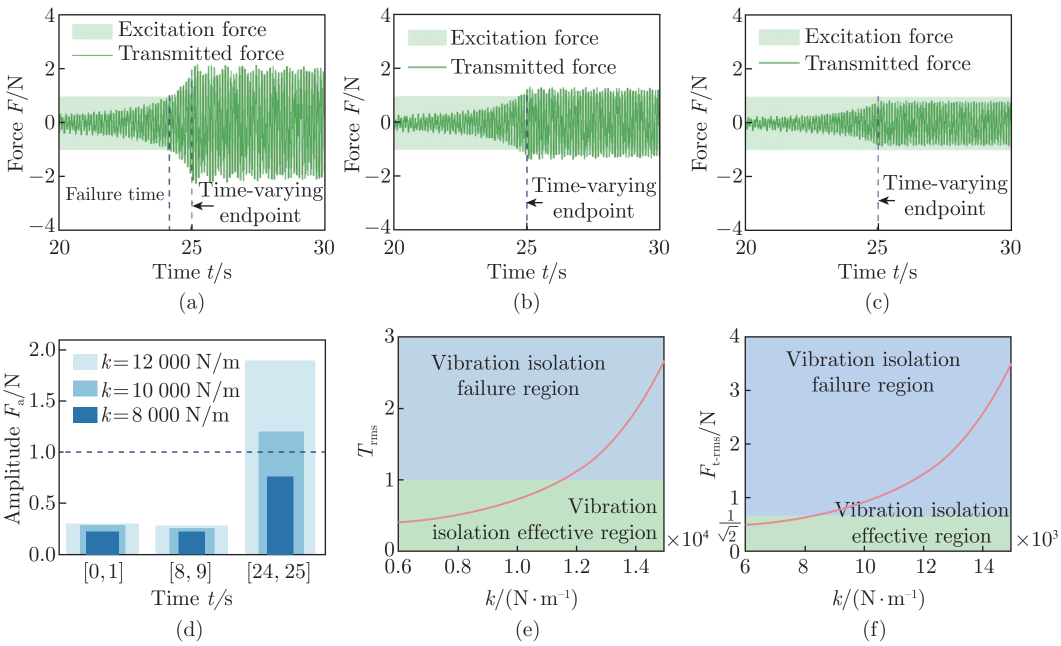

Fig. 9 Effects of system stiffness on vibration isolation effectiveness: (a)–(c) when k is 12 000 N/m, 10 000 N/m, and 8 000 N/m, respectively, the system transmits force responses within 20–30 s; (d) amplitude bar chart for three key time periods in the time-varying process (the peak value of the response within the given time range); (e) characteristic curve of RMS force transmissibility at different stiffness levels; (f) characteristic curve of RMS transmitted force after transient at different stiffness levels (color online)

Only the lowest stiffness configuration ($k = 8\,000\,\mathrm{N/m}$) maintains a sufficient frequency ratio to sustain isolation throughout the transient process.

Crucially, Figs. 9(e) and 9(f) reveal a critical distinction: the viable stiffness range for the transient phase is substantially wider than that of the final stabilized system. During the mass-varying process, the heavier instantaneous mass suppresses the natural frequency, momentarily permitting a broader range of stiffness values to remain effective. However, as the system settles into its final light-weight state, the isolation-onset frequency decreases, thereby narrowing the effective stiffness bandwidth. This implies that for time-varying systems, the design constraint is determined not merely by the transient performance, but primarily by the post-variation steady state.

Figure 10(a) presents the RMS transmissibility spectrum, confirming that the reduced stiffness broadens the effective frequency band by suppressing resonance and lowering the cut-on frequency. However, Fig. 10(b) reveals a critical constraint unique to time-varying systems: the trade-off between the isolation bandwidth and the FTT. Although increasing stiffness raises the cut-on frequency as expected in standard linear systems, it comes at the cost of a reduced FTT. This phenomenon is driven by a phase-advanced activation mechanism: a higher stiffness elevates the instantaneous natural frequency, thereby shifting the resonance crossing point earlier in the mass-decay process. Consequently, stiffer isolators narrow the temporal window of effective protection, exposing the system to resonance while the mass is still being depleted.

The temporal evolutions of these phenomena are detailed in Figs. 10(c)–10(f). In the effective isolation region (see Fig. 10(c)), the system demonstrates robustness, maintaining attenuation throughout both the transient mass depletion and the subsequent steady state without triggering an FTT event. Conversely, in the low-frequency regime (see Figs. 10(d)–10(f)), the response exhibits a distinct non-stationary amplification pattern. Driven by the shifting natural

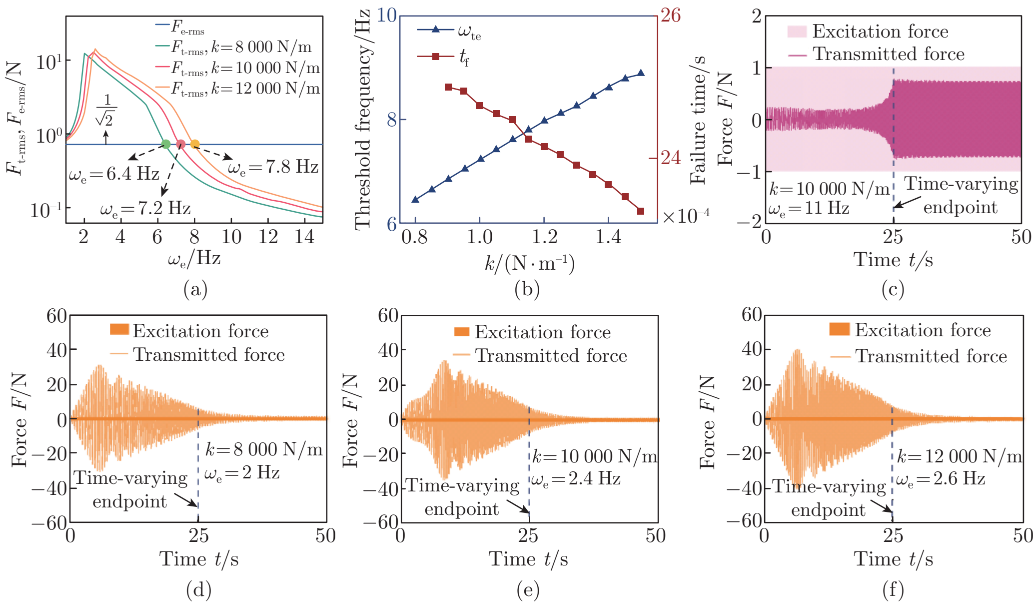

Fig. 10 Effects of excitation frequency on vibration isolation effectiveness: (a) curves of RMS values for transmitted force $F_{\mathrm{t,rms}}$ and excitation force $F_{\mathrm{e,rms}}$ as a function of excitation frequency; (b) vibration isolation threshold frequency ω_{te} and failure time t_{f} as a function of system stiffness; (c) time-domain diagram of force transmission when the vibration isolation system is active, as shown in (a); (d)–(f) complete time-domain curves of force under extreme resonance, with (d) $k = 8\,000\,\mathrm{N/m}$, $\omega_{\mathrm{e}} = 2\,\mathrm{Hz}$, (e) $k = 10\,000\,\mathrm{N/m}$, $\omega_{\mathrm{e}} = 2.4\,\mathrm{Hz}$, and (f) $k = 12\,000\,\mathrm{N/m}$, $\omega_{\mathrm{e}} = 2.6\,\mathrm{Hz}$ (color online)

frequency, the transmitted force amplitude initially increases, peaks, and then decays. Crucially, strictly distinct from transient resonance crossings, the force amplitude in the post-variation steady state remains substantially higher than that of the excitation input. This confirms that the isolator not only fails to suppress vibration during the mass change but also effectively acts as an amplifier in the final stabilized configuration, underscoring the necessity of a comprehensive design strategy that not only accounts for the terminal mass state but also strictly avoids the resonance associated with the initial mass configuration.

5 Conclusions

Time-varying mass systems constitute a pervasive yet insufficiently addressed engineering challenge, notably in applications such as rocket fuel combustion, where progressive mass depletion significantly alters the structural dynamics. This study develops a pioneering analytical framework for vibration prediction and isolation design in linear mass-dissipative systems. By adopting a parametric transformation technique, the governing time-dependent differential equations are reformulated into canonical Bessel forms, enabling closed-form solutions that are previously inaccessible for such systems. To address the computational barriers posed by non-integrable products of Bessel functions, a novel strategy is developed that combines variable upper-limit integration with grid-optimized lower bounds, effectively replacing conventional indefinite integration while preserving numerical fidelity. Building on these analytical solutions, isolation performance metrics tailored to time-varying mass systems, including transmissibility and FTT, are defined. The analysis shows that, as in constant-mass systems, isolation efficacy remains stiffness-dependent: reducing stiffness lowers the onset isolation frequency and delays or fully suppresses isolation failure during mass variation. Crucially, time-varying mass systems reveal distinctive transient behaviors absent in their steady-mass counterparts, notably amplitude modulation and abrupt isolation failure.

This study establishes a theoretical foundation for modeling mass-varying systems, predicting dynamic responses, and developing vibration isolation techniques. It extends the classical constant-mass theory to encompass parametric transient effects that are particularly relevant to real-life aerospace structures.

Conflict of interest The authors declare no conflict of interest.

References

[1] PISCHANSKYY, O. V. and VAN HORSSEN, W. T. On the nonlinear dynamics of a single degree of freedom oscillator with a time-varying mass. *Journal of Sound and Vibration*, **331**(8), 1887–1897 (2012)

[2] EKE, F. O. and MAO, T. C. On the dynamics of variable mass systems. *International Journal of Mechanical Engineering Education*, **30**(2), 123–137 (2002)

[3] ZHANG, N., CAO, G. H., ZHU, Z. C., WANG, K., and YAN, L. Nonlinear dynamics of time-varying curvature balance rope coupled with time-varying length hoisting rope in friction hoisting system. *Journal of Sound and Vibration*, **567**, 117910 (2023)

[4] CVETICANIN, L. J. The vibrations of a textile machine rotor with nonlinear characteristics. *Mechanism and Machine Theory*, **21**(1), 29–32 (1986)

[5] LEE, C. W., HAN, D. J., SUH, J. H., and HONG, S. W. Modal analysis of periodically time-varying linear rotor systems. *Journal of Sound and Vibration*, **303**(3-5), 553–574 (2007)

[6] GANJI, D. D., GORJI, M., HATAMI, M., HASANPOUR, A., and KHADEMZADEH, N. Propulsion and launching analysis of variable-mass rockets by analytical methods. *Propulsion and Power Research*, **2**(3), 225–233 (2013)

[7] CARRERA, E., CAVALLO, T., and ZAPPINO, E. Effect of solid mass consumption on the free-vibration analysis of launchers. *Journal of Spacecraft and Rockets*, **54**(3), 774–781 (2017)

[8] MEIROVITCH, L. General motion of a variable-mass flexible rocket with internal flow. *Journal of Spacecraft and Rockets*, **7**(2), 186–195 (1970)

[9] CHEN, W. T., CHEN, G. P., CHEN, T. F., TAN, X., SHAO, H. B., and HE, H. Dynamic response analysis of a typical time-varying mass system: a moving-interface pipe model, the WKB-recursive solution and experimental validation. *Applied Mathematical Modelling*, **125**, 147–166 (2024)

[10] WANG, Y. B., FANG, X. R., DING, H., and CHEN, L. Q. Quasi-periodic vibration of an axially moving beam under conveying harmonic varying mass. *Applied Mathematical Modelling*, **123**, 644–658 (2023)

[11] ZHANG, L. X., BAI, Z. F., ZHAO, Y., and CAO, X. B. Dynamic response of solar panel deployment on spacecraft system considering joint clearance. *Acta Astronautica*, **81**(1), 174–185 (2012)

[12] LI, D. X. and LIU, W. Vibration control for the solar panels of spacecraft: innovation methods and potential approaches. *International Journal of Mechanical System Dynamics*, **3**(4), 300–330 (2023)

[13] YANG, Y., TANG, J. Y., HU, N. Q., SHEN, G. J., LI, Y. H., and ZHANG, L. Research on the time-varying mesh stiffness method and dynamic analysis of cracked spur gear system considering the crack position. *Journal of Sound and Vibration*, **548**, 117505 (2023)

[14] ZHANG, W., GAO, Y. H., and LU, S. F. Theoretical, numerical and experimental researches on time-varying dynamics of telescopic wing. *Journal of Sound and Vibration*, **522**, 116724 (2022)

[15] LIAO, F. L., HUANG, J. L., and ZHU, W. D. Investigation on nonlinear vibration of a gear transmission system considering time-varying mesh stiffness and time-varying supporting stiffness. *Journal of Sound and Vibration*, **603**, 118957 (2025)

[16] SHI, J. F., GOU, X. F., and ZHU, L. Y. Five-state engaging model and dynamics of gear-rotor-bearing system based on time-varying contact analysis considering gear temperature and lubrication. *Applied Mathematical Modelling*, **112**, 47–77 (2022)

[17] XIANG, L., JIA, Y., and HU, A. J. Bifurcation and chaos analysis for multi-freedom gear-bearing system with time-varying stiffness. *Applied Mathematical Modelling*, **40**(23-24), 10506–10520 (2016)

[18] MA, H., GUAN, H., QU, L., GUO, X. M., MU, Q. Q., ZENG, Y., and CHEN, Y. Y. Dynamic modeling and simulation of blade-casing system with rubbing considering time-varying stiffness and mass of casing. *Applied Mathematics and Mechanics* (*English Edition*), **46**(5), 849–868 (2025) https://doi.org/10.1007/s10483-025-3244-7

[19] LIU, K. Identification of linear time-varying systems. *Journal of Sound and Vibration*, **206**(4), 487–505 (1997)

[20] BARTFAI, A., PONCE-VANEGAS, F. E., HOGAN, S. J., KUSKE, R., and DOMBOVARI, Z. Semi-analytical framework for the study of finite-time stability of forced dynamical systems with slowly varying parameters. *Journal of Sound and Vibration*, **618**, 119359 (2025)

[21] LI, C. Y., HAO, J., LIU, H. W., HUA, C. L., and YAO, Z. H. Nonlinear parametric vibration and stability analysis of worm drive system with time-varying meshing stiffness and backlash. *Journal of Sound and Vibration*, **575**, 118264 (2024)

[22] BISAILLON, P., ROBINSON, B., KHALIL, M., PETTIT, C. L., POIREL, D., and SARKAR, A. Robust Bayesian state and parameter estimation framework for stochastic dynamical systems with combined time-varying and time-invariant parameters. *Journal of Sound and Vibration*, **575**, 118106 (2024)

[23] WEI, S., CHEN, S. Q., DONG, X. J., PENG, Z. K., and ZHANG, W. M. Parametric identification of time-varying systems from free vibration using intrinsic chirp component decomposition. *Acta Mechanica Sinica*, **36**(1), 188–205 (2020)

[24] HOZHABROSSADATI, S. M. and SANI, A. A. Free vibration of MDOF systems with nonperiodically time-varying mass. *International Journal of Structural Stability and Dynamics*, **18**(6), 1850077 (2018)

[25] LI, Q. S. Free vibration of SDOF systems with arbitrary time-varying coefficients. *International Journal of Mechanical Sciences*, **43**(3), 759–770 (2001)

[26] LI, Q. S., FANG, J. Q., and LIU, D. K. Exact solutions for free vibration of single-degree-of-freedom systems with nonperiodically varying parameters. *Journal of Vibration and Control*, **6**(3), 449–462 (2000)

[27] NHLEKO, S. Free vibration states of an oscillator with a linear time-varying mass. *Journal of Vibration and Acoustics*, **131**(5), 051011 (2009)

[28] LI, Q. S. A new exact approach for analyzing free vibration of SDOF systems with nonperiodically time varying parameters. *Journal of Vibration and Acoustics*, **122**(2), 175–179 (2000)

[29] LI, Q. S. Forced vibrations of single-degree-of-freedom systems with nonperiodically time-varying parameters. *Journal of Engineering Mechanics*, **128**(12), 1267–1275 (2002)

[30] LIU, M., LI, Z., YANG, X. D., ZHANG, W., and LIM, C. W. Dynamic analysis of a deployable/retractable damped cantilever beam. *Applied Mathematics and Mechanics* (*English Edition*), **41**(9), 1321–1332 (2020) https://doi.org/10.1007/s10483-020-2650-6

[31] LI, J., ZHANG, R. S., and TIMOSHIN, S. A. Asymptotically almost periodic solutions for time-varying integro-differential inclusions with nonlocal conditions. *Communications in Nonlinear Science and Numerical Simulation*, **152**, 109229 (2026)

[32] SRINIVASAN, P. and SANKAR, T. S. A study of linear systems with time varying coefficients by the methods of Bessel and Weber functions. *Journal of Sound and Vibration*, **37**(3), 297–309 (1974)

[33] LI, Q. S. Analytical evaluation of dynamic responses of time-varying systems. *Journal of Vibration and Control*, **15**(8), 1123–1142 (2009)

[34] ZUKOVIC, M. and KOVACIC, I. An insight into the behaviour of oscillators with a periodically piecewise-defined time-varying mass. *Communications in Nonlinear Science and Numerical Simulation*, **42**, 187–203 (2017)

[35] FU, J., BAI, J. F., LAI, J. J., LI, P. D., YU, M., and LAM, H. K. Adaptive fuzzy control of a magnetorheological elastomer vibration isolation system with time-varying sinusoidal excitations. *Journal of Sound and Vibration*, **456**, 386–406 (2019)

[36] DUAN, X. F., YE, J. M., HUANG, D. M., and DENG, H. Investigation of dynamical behaviors of bionic paw-inspired vibration isolators by theoretical and numerical analysis. *International Journal of Dynamics and Control*, **13**(12), 399 (2025)

[37] ZHENG, H. B., QIN, H., REN, M. K., and ZHANG, Z. Y. Active vibration control for the time-varying systems with a new adaptive algorithm. *Journal of Vibration and Control*, **26**(3-4), 200–213 (2020)

[38] LIU, F. H., YU, D. Y., WANG, C., and WANG, G. Y. Advances in variable stiffness vibration isolator and its application in spacecraft. *International Journal of Structural Stability and Dynamics*, **22**(13), 2230004 (2022)

[39] ZHAO, L., LU, Z. Q., DING, H., and CHEN, L. Q. A viscoelastic metamaterial beam for integrated vibration isolation and energy harvesting. *Applied Mathematics and Mechanics* (*English Edition*), **45**(7), 1243–1260 (2024) https://doi.org/10.1007/s10483-024-3159-7

[40] CHEN, T. T., WANG, K., WANG, Q., WANG, Y. D., CHENG, L., and ZHOU, J. X. A Chinese lantern-inspired low frequency energy harvester with synchronized multi-branched conversion elements. *Engineering Structures*, **334**, 120266 (2025)

[41] SHU, Y. Q., WANG, K., CHEN, T. T., PAN, H. B., DENG, Y. P., YIN, H. F., and ZHOU, J. X. A quasi-zero-stiffness metastructure for concurrent low-frequency vibration attenuation and energy harvesting. *Thin-Walled Structures*, **214**, 113371 (2025)

[42] CHEN, T. T., DING, Y., XU, Z. Y., WANG, K., ZHOU, J. X., and CHANG, Y. P. Bidirectional vibration energy harvesting and sensing system with biomimetic petal architecture. *Renewable Energy*, **256**, 124614 (2026)

[43] LI, M. and DING, H. A vertical track nonlinear energy sink. *Applied Mathematics and Mechanics* (*English Edition*), **45**(6), 931–946 (2024) https://doi.org/10.1007/s10483-024-3127-6

[44] ZENG, Y. C., DING, H., and JI, J. C. An origami-inspired nonlinear energy sink: design, modeling, and analysis. *Applied Mathematics and Mechanics* (*English Edition*), **46**(4), 601–616 (2025) https://doi.org/10.1007/s10483-025-3239-6

[45] HU, Y., ZHANG, H. C., WANG, K., FANG, Y. G., and MA, C. H. Analytical analysis of vibration isolation characteristics of quasi-zero stiffness suspension backpack. *International Journal of Dynamics and Control*, **12**(12), 4387–4397 (2024)

[46] YANG, T., ZHOU, S. X., FANG, S. T., QIN, W. Y., and INMAN, D. J. Nonlinear vibration energy harvesting and vibration suppression technologies: designs, analysis, and applications. *Applied Physics Reviews*, **8**(3), 031317 (2021)

[47] ZHOU, S. X., LALLART, M., and ERTURK, A. Multistable vibration energy harvesters: principle, progress, and perspectives. *Journal of Sound and Vibration*, **528**, 116886 (2022)

[48] CHEN, T. T., WANG, K., CHEN, S. C., XU, Z. Y., LI, Z., and ZHOU, J. X. Nonlinear electromechanical coupling dynamics of a two-degree-of-freedom hybrid energy harvester. *Applied Mathematics and Mechanics* (*English Edition*), **46**(6), 989–1010 (2025) https://doi.org/10.1007/s10483-025-3264-7

[49] ZHOU, J. H., ZHOU, J. X., PAN, H. B., WANG, K., CAI, C. Q., and WEN, G. L. Multi-layer quasi-zero-stiffness meta-structure for high-efficiency vibration isolation at low frequency. *Applied Mathematics and Mechanics* (*English Edition*), **45**(7), 1189–1208 (2024) https://doi.org/10.1007/s10483-024-3157-6

[50] YU, Y. H., ZHANG, X. C., and LI, F. M. Reducing vibration isolation frequency in an X-shaped two-stage nonlinear system. *Communications in Nonlinear Science and Numerical Simulation*, **135**, 108080 (2024)

[51] ZHANG, Q., YANG, Y. H., HOU, T., and ZHANG, R. J. Dynamic analysis of high-speed traction elevator and traction car-rope time-varying system. *Noise & Vibration Worldwide*, **50**(2), 37–45 (2019)

[52] PENG, Q. F., XU, P., YUAN, H., MA, H. X., XUE, J. H., HE, Z. Y., and LI, S. Q. Analysis of vibration monitoring data of flexible suspension lifting structure based on time-varying theory. *Sensors*, **20**(22), 6586 (2020)

[53] YANG, J. S., XIE, J. S., CHEN, G. G., and CHEN, J. L. An efficient method for vibration equations with time varying coefficients and nonlinearities. *Journal of Low Frequency Noise, Vibration and Active Control*, **40**(4), 1744–1763 (2021)

[54] WANG, J. H., LIU, J., and PAN, G. A time-domain piecewise calculation method of a time-varying isolation platform. *Mechanical Systems and Signal Processing*, **228**, 112416 (2025)

[55] WANG, K., ZHOU, J. X., TAN, D. G., LI, Z. Y., LIN, Q. D., and XU, D. L. A brief review of metamaterials for opening low-frequency band gaps. *Applied Mathematics and Mechanics* (*English Edition*), **43**(7), 1125–1144 (2022) https://doi.org/10.1007/s10483-022-2870-9

[56] HUANG, J. H. and ZHOU, X. M. A time-varying mass metamaterial for non-reciprocal wave propagation. *International Journal of Solids and Structures*, **164**, 25–36 (2019)

[57] ENGHETA, N. Four-dimensional optics using time-varying metamaterials. *Science*, **379**(6638), 1190–1191 (2023)

[58] HUANG, J. H. and ZHOU, X. M. Non-reciprocal metamaterials with simultaneously time-varying stiffness and mass. *Journal of Applied Mechanics*, **87**(7), 071003 (2020)

[59] LIU, Z. Y., YI, K. J., SUN, H. P., ZHU, R., ZHOU, X. M., HU, G. K., and HUANG, G. L. Inherent temporal metamaterials with unique time-varying stiffness and damping. *Advanced Science*, **11**(43), 2404695 (2024)

[60] HOLL, H. J., BELYAEV, A. K., and IRSCHIK, H. Simulation of the Duffing-oscillator with time-varying mass by a BEM in time. *Computers & Structures*, **73**(1-5), 177–186 (1999)

[61] FLORES, J., SOLOVEY, G., and GIL, S. Variable mass oscillator. *American Journal of Physics*, **71**(7), 721–725 (2003)

[62] YONEZAWA, A., YONEZAWA, H., and KAJIWARA, I. Vibration control for various structures with time-varying properties via model-free adaptive controller based on virtual controlled object and SPSA. *Mechanical Systems and Signal Processing*, **170**, 108801 (2022)

[63] JEONG, H. K., HAN, J. H., YOUN, S. H., and LEE, J. Frequency tunable vibration and shock isolator using shape memory alloy wire actuator. *Journal of Intelligent Material Systems and Structures*, **25**(7), 908–919 (2014)

[64] PARK, Y. H., KWON, S. C., KOO, K. R., and OH, H. U. High damping passive launch vibration isolation system using superelastic SMA with multilayered viscous lamina. *Aerospace*, **8**(8), 201 (2021)